International Journal of Modern Physics C
Vol. 30, No. 4 (2019) 1950026 (17 pages)

DOI: 10.1142/S0129183119500268

Periodic orbit scar in wavepacket propagation

Mitsuyoshi Tomiya* and Shoichi Sakamoto†

Faculty of Science and Technology
Seikei University, Kichijyoji-Kitamachi 3-3-1
Musashino-shi, Tokyo 180-8633, Japan
**tomiya@st.seikei.ac.jp*
†*sakamoto@st.seikei.ac.jp*

Eric J. Heller

Department of Physics
Harvard University, Cambridge
Massachusetts 02138, USA
heller@physics.harvard.edu

Received 26 November 2017
Accepted 15 March 2019
Published 24 April 2019

This study analyzed the scar-like localization in the time-average of a time-evolving wavepacket on a desymmetrized stadium billiard. When a wavepacket is launched along the orbits, it emerges on classical unstable periodic orbits as a scar in stationary states. This localization along the periodic orbit is clarified through the semiclassical approximation. It essentially originates from the same mechanism of a scar in stationary states: piling up of the contribution from the classical actions of multiply repeated passes on a primitive periodic orbit. To achieve this, several states are required in the energy range determined by the initial wavepacket.

Keywords: Scar states; wavepackets; semiclassical approximation.

PACS Nos.: 05.45.Mt, 03.65.Sg, 05.45.Ac.

1. Introduction

This study investigates localization in the time-average of the absolute squares of the time-evolving wave function on a desymmetrized stadium billiard that occurs after a Gaussian wavepacket is launched as an initial state. In chaotic billiards such as a stadium, nodal patterns of stationary states with unique characteristics were discovered approximately three decades ago.[1] The patterns often have a unique enhancement along classical unstable periodic orbits. Such a phenomenon is called scar in quantum stationary states of a finite chaotic region. The eigen states with scars are called scar states. In contrast, in integrable billiards, the nodal patterns

*Corresponding author.

are essentially repetitive and synthetic. The eigen states are a genuine quantum mechanical concept, whereas the periodic orbits are apparently classical mechanical objects. The scar state is an important discovery expressing a providential quantum classical correspondence.

A semiclassical approximation emerged as a powerful tool to determine scar states in quantum systems along the classical unstable periodic orbits. This method has been used to construct theories of scars in coordinate space[2] and phase space[3,4]; they successfully clarify the contribution of the periodic orbits to the scar states. Both theories discuss the energy dependence of scars because the scars are first discovered in the eigen states. Bogomolny[2] proposed the Green's function in terms of the actions of the classical periodic orbits to expose the periodic orbits as the origins of the scar in the coordinate space. Berry's theory[4] utilizes the Wigner function under approximation in the phase space to determine the cause of the scars. In particular, Heller's lecture[3] revealed the dynamical properties of scars, stating that the time-evolving wavepackets propagate near the periodic orbits. In particular, the Heller group focused on homoclinic orbits and the return of the Gaussian wavepacket to the neighborhood of its launching point in finite regions. In addition, they realized the importance of the autocorrelation function and its Fourier counterpart — the weighted spectrum.[5–9]

Finally, the enhancement or localization in the time-average of a time-evolving wavepacket was discovered.[10,11] In this study, it is called as the "dynamical scar."

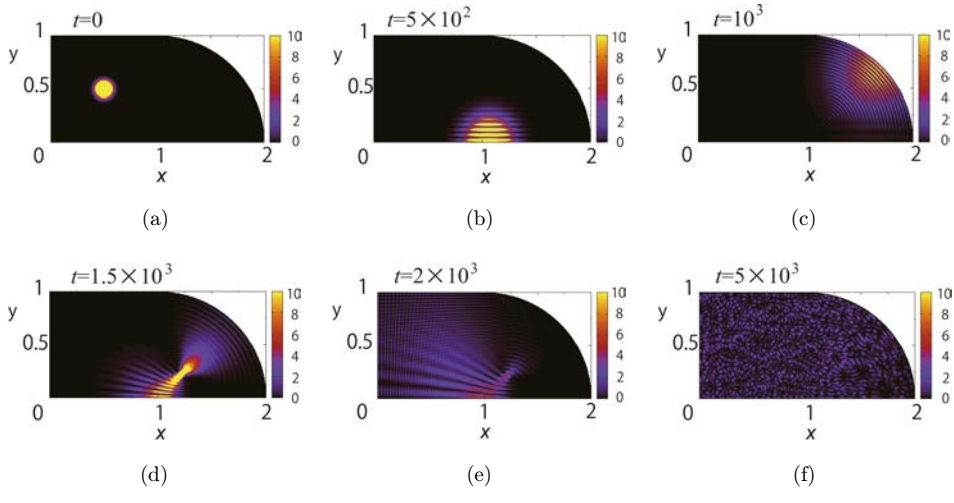

Fig. 1. (Color online) (a)–(f) Illustrations of time-evolution of the Gaussian wavepacket $|\Psi(t)|^2$ in a desymmetrized stadium billiard. The initial packet Ψ_0 is as Eq. (2). The x-coordinate is set along the bottom line of the stadium, and the y-coordinate is on the left straight boundary. Thus, the origin of the coordinate is located on the bottom-left corner. The wavepacket is launched from $\mathbf{r}_0 = (1/2, 1/2)$ and travels with a launching angle $\theta = -\pi/4$(a), which is defined in the counterclockwise direction from the direction of the x-axis, $|\mathbf{p}_0| = 250$ and $\sigma_0 = 0.15$. The orbit corresponds to the periodic orbit No. 7 in Ref. 2. After approximately $t = 5 \times 10^3$, the wave function defuses almost all over the stadium(f).

It has a distinctly close relation to scar states because it also emerges along a periodic orbit.[12] The scar states are also shown to contribute significantly to the dynamical states. The window function[13] for the semiclassical approximation to describe the enhancement is derived from a weighted power spectrum.

However, it is known that the reflection symmetries of the billiard's shape sometimes prevent the detection of its genuine chaotic characteristics. To remove the discrete symmetries, we studied the localization in a desymmetrized 2×4 stadium billiard.[14] The desymmetrization eliminates two discrete mirror symmetries of a full stadium shape and makes the chaotic properties more evident. We use Table I in Ref. 2 to distinguish the periodic orbits; however, the table is pertaining to a full stadium, and is not for a desymmetrized stadium. Therefore, it should be used with caution. If the periodic orbits pass over the horizontal and vertical axes of the symmetries, they may have to be folded at the crossing points for the desymmetrized stadium (cf. Figs. 2 and 3). Then, we can specify the periodic orbit with "No." in the table. For example, in Fig. 1, the periodic orbit which the Gaussian wavepacket travels along is called No. 7.

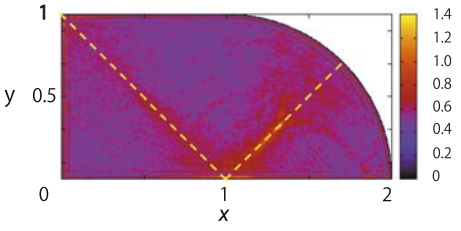

Fig. 2. (Color online) The time-average of the evolving wavepacket $A(\mathbf{r})$ in Fig. 1. The weak concentration appears along the broken yellow lines, which represents the corresponding unstable periodic orbit. It shows the shape of the desymmetrized orbit No. 7.

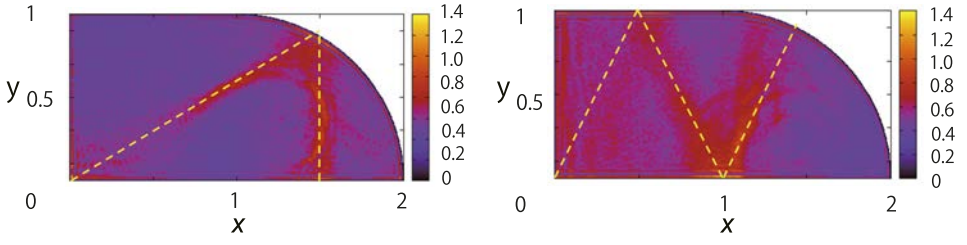

Fig. 3. (Color online) The time-averages of the evolving wavepackets $A(\mathbf{r})$ in stadium billiard with different initial conditions. In both cases for the initial Gaussian wavepackets, $|\mathbf{p}_0| = 250$ and $\sigma_0 = 0.15$. (a) The wavepacket is launched from $(1/2, \sqrt{3}/6)$ and its launching angle is $\theta = \pi/6$. This shows the shape of the desymmetrized orbit No. 12. (b) The wavepacket launched from $(1/4, 1/2)$ has an angle defined as $\tan\theta = 2$. This corresponds to orbit No. 14. The launching angles are defined as those in Fig. 1. The broken yellow lines correspond to the classical unstable periodic orbits.

2. Gaussian Wavepacket as a Probe for Dynamical Properties

The time-dependent Schrödinger equation

$$i\hbar\frac{\partial\Psi}{\partial t} = -\frac{\hbar^2}{2m}\nabla^2\Psi + V\Psi \tag{1}$$

governs the dynamical properties of the quantum systems, considering a particle of mass m. By adopting the quarter of the 2×4 stadium (Figs. 1–3) as a two-dimensional (2D) chaotic finite structure, the potential is simply set as $V = 0$ inside the billiard and $V = \infty$ outside of it.

The Gaussian wavepacket is a conventional tool used for elucidating the time-evolution of quantum states.[6–9] It has been one of the fundamental quantum objects since the early stage of quantum mechanics. Its initial form in a 2D region is

$$\Psi_0(\mathbf{r}) = \frac{1}{\sigma_0\sqrt{\pi}}\exp\left[\frac{i}{\hbar}\mathbf{p}_0(\mathbf{r}-\mathbf{r}_0) - \frac{(\mathbf{r}-\mathbf{r}_0)^2}{2{\sigma_0}^2}\right], \tag{2}$$

where $\mathbf{r} = (x, y)$ is a point inside the nanostructure, $\mathbf{r_0} = (x_0, y_0)$ is the initial location of the center of the wavepacket, and $\mathbf{p}_0 = (p_{0x}, p_{0y})$ is the packet's initial momentum. The standard deviation of the Gaussian packet σ_0 determines its size.

If the Gaussian wavepacket is placed in a flat infinite space, it travels as a bunch with the initial velocity of the center of the wavepacket $\mathbf{v}_0 = \mathbf{p}_0/m$. The absolute value of the wavepacket shows that its shape is always Gaussian; however, its size increases as $|\sigma(t)| = \sigma_0\sqrt{1 + (\frac{\hbar t}{m{\sigma_0}^2})^2}$. If the time is sufficiently long, $\sigma(t) \approx \frac{\hbar}{m\sigma_0}t$.

In this work, the wavepacket travels in the finite region, and repeated reflections on the boundary eventually diffuse it around the billiard (Fig. 1; also see Refs. 10 and 11). Initially it behaves like a viscous liquid. The specific texture of the traveling wavepacket then gradually and progressively decreases. Finally, in the chaotic billiards, the snapshots of wave function ripple over the billiard with irregular granular pattern. On the contrary, the autocorrelation function surprisingly exhibits long-time recurrence.[7] This also implies the localization on the periodic orbit.

3. Dynamical Scar

One of the most fundamental concepts in quantum physics is the use of the absolute square of the wave function to derive any physical properties; usually its time-average is important to investigate the quantum effect. Therefore, the time-average of the absolute square of the wave function is as follows:

$$A_T(\mathbf{r}) = \frac{1}{T}\int_0^T |\Psi(\mathbf{r}, t)|^2 dt. \tag{3}$$

This is an appropriate tool to detect the desirable localization. Here, T expresses the time required to measure the time-average.

For numerical calculation, it is discretized as

$$A_T(\mathbf{r}_i) = \frac{1}{N_t}\sum_{j=0}^{N_t} |\Psi(\mathbf{r}_i, t_j)|^2, \tag{4}$$

on the mesh points $\mathbf{r}_i = (x_i, y_i)$, and the integration over time is the summation over the discretized times $t_j = j\Delta t$, where Δt is a time step. The summation must then be divided by the integer N_t representing the number of whole time steps and apparently $T = N_t\Delta t$. In this study, the natural units $\hbar = m = 1$ are always applied for actual numerical evaluation. The time step is set at $\Delta t = 2.5 \times 10^{-2}$, $T = 9 \times 10^4$, or $N_t = 3.6 \times 10^6$, and the lattice constant is 0.2. A typical example of the calculated A_T is presented in Fig. 2. The time-average expresses clear localization along unstable periodic orbits despite no specific patterns in the snapshots of the wavepackets (e.g. Fig. 1(f)).

It is apparently similar to the scars in stationary wave functions[1] Furthermore, different launching conditions exhibit the same phenomena on various periodic orbits, as shown in Fig. 3 (also see Ref. 12). The enhancement appears clearly around the periodic orbit if the initial location of the center of the wavepacket and its velocity are on and along the orbit. These are referred to as "dynamical scars" to distinguish them from the scar states in stationary eigen states. These are enhancements in the time-average of the time-dependent wave function.

Any states in the quantum systems can be expanded using these eigenfunctions as

$$\Psi(\mathbf{r}, t) = \sum_n c_n\psi_n(\mathbf{r}, t) = \sum_n c_n\phi_n(\mathbf{r})\exp\left(-\frac{i}{\hbar}E_n t\right), \tag{5}$$

where $\psi_n(\mathbf{r}, t) = \phi_n(\mathbf{r})\exp(-\frac{i}{\hbar}E_n t)$ is the nth eigen state of the system with energy E_n. The expansion coefficient c_n must satisfy the condition $\sum_n |c_n|^2 = 1$. In this study, the initial state is set as $\Psi(\mathbf{r}, t = 0) = \Psi_0(\mathbf{r})$. The expansion coefficient c_n can be determined using the initial wavepacket Ψ_0 as

$$c_n = \int \phi_n^*\Psi_0(\mathbf{r})d\mathbf{r}. \tag{6}$$

Moreover, the expansion can be used to elucidate the time-average of $|\Psi(\mathbf{r}, t)|^2$ as

$$\begin{aligned} A(\mathbf{r}) &= \lim_{T\to\infty} A_T(\mathbf{r}) = \lim_{T\to\infty}\frac{1}{T}\int_0^T |\Psi(\mathbf{r}, t)|^2 dt \\ &= \lim_{T\to\infty}\frac{1}{T}\int_0^T \left[\sum_n |c_n|^2|\phi_n(\mathbf{r})|^2 + \sum_{n\neq m} c_m^* c_n\phi_m^*\phi_n \exp\left\{\frac{i}{\hbar}(E_m - E_n)t\right\}\right] dt \\ &= \sum_n |c_n|^2|\phi_n(\mathbf{r})|^2, \end{aligned} \tag{7}$$

assuming $E_n \neq E_m$, if $n \neq m$. In other words, using Eq. (7), if the coefficients c_n of the scar eigen states on the same periodic orbit have dominantly larger values, the "dynamical scars" of the periodic orbits are observed in the time-average $A(\mathbf{r})$.[10–12]

Therefore, at least theoretically, the time-average (7) can be written in energy integration as follows:

$$A(\mathbf{r}) = \int \sum_n |c_n|^2 |\phi_n(\mathbf{r})|^2 \delta(E - E_n) dE. \tag{8}$$

However, the Dirac delta function must be treated carefully to allow comparison of numerical results and experimental data. The behavior of the delta functions is often smoothed by the limitation of the precision of numerical calculation and experimental measurement.

Equation (8) can be considered as the summation of the related wave functions and the specific contribution weight that closely corresponds to the weighted spectrum because it includes the factor $|c_n|^2$. In the numerical calculation, the weighted spectrum would be smoothed by the numerical discretization and the precision of the calculation. The Dirac delta function could be replaced with a smoothed function.

4. Window Function

The correlation function between the traveling wavepacket (5) and initial state (2) $C_0(t) = \int \Psi_0^*(\mathbf{r})\Psi(\mathbf{r}, t) d\mathbf{r}^2$ closely relates to the weighted spectrum. The autocorrelation function is expressed by the eigenfunction expansion (5) as

$$\begin{aligned} C_0(t) &= \int \Psi_0^*(\mathbf{r})\Psi(\mathbf{r}, t) d^2\mathbf{r} \\ &= \int \left(\sum_m c_m^* \phi_m^* \right) \left(\sum_n c_n \phi_n e^{-\frac{i}{\hbar} E_n t} \right) d^2\mathbf{r} \\ &= \sum_n |c_n|^2 e^{-\frac{i}{\hbar} E_n t}. \end{aligned} \tag{9}$$

The weighted spectrum can be defined through its Fourier transform as

$$\begin{aligned} \tilde{C}_0(E) &= \frac{1}{2\pi} \int_{-\infty}^{\infty} C_0(t) e^{\frac{i}{\hbar} E t} dt \\ &= \frac{1}{2\pi} \int_{-\infty}^{\infty} \sum_n |c_n|^2 e^{\frac{i}{\hbar}(E - E_n)t} dt \\ &= \hbar \sum_n |c_n|^2 \delta(E - E_n) \\ &= \hbar P(E). \end{aligned} \tag{10}$$

This only represents the bare weighted power spectrum $P(E) = \sum_n |c_n|^2 \delta(E - E_n)$ with the Planck's constant.

The smoothed version of the weighted spectrum and the Green's function produce a neat form of the time-average. The smoothed weighted spectrum function (SWSF) can be written as

$$P_\epsilon(E) = \sum_n |c_n|^2 \delta_\epsilon(E - E_n). \tag{11}$$

In addition, we have $\lim_{\epsilon\to 0} P_\epsilon(E) = P(E)$. When ϵ becomes infinitesimal, $\lim_{\epsilon\to 0}\delta_\epsilon(x) = \delta(x)$. Here, the Lorentzian form of the smoothed version delta function is introduced as

$$\delta_\epsilon(E - E_n) = \frac{\epsilon}{\pi}\frac{1}{(E - E_n)^2 + \epsilon^2}. \tag{12}$$

Realistic systems have finite precision and always show errors because of numerical applications, limit of measurement, etc. Owing to these inevitable limitations of the systems, the Dirac delta functions are replaced by some finite regular functions. Its infinity and singular behavior cannot be recreated exactly through computation; they seem very large but are finite and singular-like; however, the peaks are not numerically infinite. The width of the Lorentzian ϵ will be the order of the mean level spacing $\overline{\Delta E}$ under such limitation because much finer energy difference would not be distinguishable. The replacement is allowed if the width of the Lorentzian ϵ is equal or larger than the order of the mean level spacing $\overline{\Delta E}$. By using this expression, the smoothed Green's function

$$\mathrm{Im}G_\epsilon(\mathbf{r}, \mathbf{r}; E) = -\pi\sum_n |\phi_n(\mathbf{r})|^2\delta_\epsilon(E - E_n) \tag{13}$$

is also introduced.

Under such circumstances, a square of the delta functions can be treated using the Berry's method.[15] The smoothed delta function (12) has a remarkable property:

$$\bar{\delta_\epsilon}(E - E_n) = 2\pi\epsilon[\delta_\epsilon(E - E_n)]^2 = \frac{2\epsilon^3}{\pi}\frac{1}{\{(E - E_n)^2 + \epsilon^2\}^2}, \tag{14}$$

where $\bar{\delta_\epsilon}(E - E_n)$ is another version of the smoothed delta function $\lim_{\epsilon\to 0}\bar{\delta_\epsilon}(x) = \delta(x)$. Next, we use an alternative practical version of the time-average

$$A_\epsilon(\mathbf{r}) = \int\sum_n |c_n|^2|\phi_n(\mathbf{r})|^2\,\bar{\delta_\epsilon}(E - E_n)dE. \tag{15}$$

The original time-average A is in the limit $A(\mathbf{r}) = \lim_{\epsilon\to 0}A_\epsilon(\mathbf{r})$.

By multiplying the two terms (11) and (13), we obtain

$$\begin{aligned}
&P_\epsilon(E)\mathrm{Im}G_\epsilon(\mathbf{r}, \mathbf{r}; E)\\
&\quad= \sum_n |c_n|^2\delta_\epsilon(E - E_n)\left\{-\pi\sum_{n'} |\phi_{n'}(\mathbf{r})|^2\delta_\epsilon(E - E_{n'})\right\}\\
&\quad= -\pi\sum_{n,n'} |c_n|^2|\phi_{n'}(\mathbf{r})|^2\delta_\epsilon(E - E_n)\delta_\epsilon(E - E_{n'})\\
&\quad= -\pi\sum_n |c_n|^2|\phi_n(\mathbf{r})|^2[\delta_\epsilon(E - E_n)]^2\\
&\quad= \frac{-1}{2\epsilon}\sum_n |c_n|^2|\phi_n(\mathbf{r})|^2\,\bar{\delta_\epsilon}(E - E_n).
\end{aligned} \tag{16}$$

Here, Eq. (14) is also applied for this deformation. Finally, Eq. (16) is used to provide the following expression for the time-average by using the Green's function

$$\begin{aligned} A_\epsilon(\mathbf{r}) &= -2\epsilon \int_{-\infty}^{\infty} P_\epsilon(E) \mathrm{Im} G_\epsilon(\mathbf{r},\mathbf{r};E) dE \\ &= \int_{-\infty}^{\infty} w(E) \mathrm{Im} G_\epsilon(\mathbf{r},\mathbf{r};E) dE, \end{aligned} \tag{17}$$

where the window function $w(E)$ is introduced[13] through SWSF (11) as

$$w(E) = -2\epsilon P_\epsilon(E) = -\frac{2\epsilon}{\hbar}\tilde{C_0}(E). \tag{18}$$

In other words, $w(E)$ is the weight for the integration over the energy region to evaluate the time-average $A_\epsilon(E)$ from the imaginary part of the smoothed Green's function (13). This specific quantum phenomenon has been focused upon in this study. It determines where the window should be transparent in the energy spectrum.

In a 2D flat and infinite space, the traveling wavepacket can be calculated exactly. The autocorrelation function is then well approximated as

$$C_f(t) = \int \Psi_0^*(\mathbf{r})\Psi(\mathbf{r},t) d^2\mathbf{r} \approx \exp\left(-\frac{v^2t^2}{4\sigma_0^2} - \frac{i}{\hbar}E_0 t\right), \tag{19}$$

and its real phase part

$$C_R(t) \approx \exp\left(-\frac{v^2t^2}{4\sigma_0^2}\right) \tag{20}$$

satisfactorily represents the damping behavior of the correlation function $C_f(t)$.

In a chaotic finite region, the autocorrelation function should differ as

$$C(t) \approx \sum_n \exp\left\{-\frac{v^2(t-n\tau)^2}{4\sigma_0^2} - \frac{i}{\hbar}E_0(t-n\tau)\right\}\exp\left(-\frac{\lambda}{2}|t|\right), \tag{21}$$

where τ is the period of a particular periodic orbit, along which the initial wavepacket is launched.[3] The summation implies that the finite region allows the wavepacket to repeatedly return to its original location. Moreover, its chaoticity makes it spread all over the billiard exponentially under the Lyapunov exponent λ of the periodic orbit. It can be reformed using the Poisson summation rule as

$$C(t) = \sum_n \frac{1}{\hbar}\frac{\Delta}{\sqrt{\pi}}\frac{\sigma_0}{v}\exp\left\{-\frac{\sigma_0^2}{v^2\hbar^2}(E_n - E_0)^2\right\} e^{-\frac{i}{\hbar}E_n t} e^{-\frac{\lambda}{2}|t|}, \tag{22}$$

where $E_n \simeq E_p + \Delta n$ and $E_0 = \frac{\mathrm{p_0}^2}{2m}$. Here, E_p represents the energy at the highest maximum of the serial local peaks with width λ and $\Delta = 2\pi\hbar/\tau (= \hbar\omega)$ is the energy gap between the local peaks. The weighted power spectrum can then be derived

through the Fourier transform of the autocorrelation function (22) as follows:

$$\begin{aligned}\tilde{C}(E) &= \frac{1}{2\pi}\int_{-\infty}^{\infty} C(t)e^{\frac{i}{\hbar}Et}dt \\ &= \sum_{n=-\infty}^{\infty}\frac{1}{\hbar}\frac{\Delta}{\sqrt{\pi}}\frac{\sigma_0}{v}\exp\left\{-\frac{\sigma_0^2}{v^2\hbar^2}(E_n-E_0)^2\right\}\times\frac{1}{\pi}\frac{\lambda/2}{((E-E_n)/\hbar)^2+(\lambda/2)^2}.\end{aligned} \tag{23}$$

This also includes the Lorentzian function of (12); however, the origin of its peaky behavior is completely different from ϵ. The Lyapunov exponent λ is purely due to the chaotic property of our system and does not exist in $C_f(t)$.

Therefore, replacing $\tilde{C}_0(E)$ with $\tilde{C}(E)$, the relationship between the window function and power spectrum should be modified to

$$w(E) \cong -\frac{2\epsilon}{\hbar}\tilde{C}(E). \tag{24}$$

Then, by Eq. (23), the window function is expected to be

$$\begin{aligned}w(E) \approx\ & -2\epsilon\frac{1}{\sqrt{\pi}}\frac{\sigma_0}{v}\exp\left\{-\frac{\sigma_0^2}{v^2\hbar^2}(E-E_0)^2\right\} \\ & \times\frac{\Delta}{\pi}\sum_{n=-\infty}^{+\infty}\frac{\lambda/2}{(E-E_p-n\Delta)^2+(\hbar\lambda/2)^2}.\end{aligned} \tag{25}$$

The interplay of the Gaussian envelope shape with its width $v\hbar/\sigma_0$ is due to the size of the initial Gaussian (1) and the narrow peaks, with width λ, represented by the Lorentzian. Finally, $w(E)$ is well estimated through Eq. (25) by replacing the eigen energies E_n of the eigenstates in the exponential function of Eq. (23) with an ordinary energy variable E. In reality, the resulting numerical difference of $w(E)$ is slight after the replacement. Then, the exponential function goes out form the summation symbol, and Eq. (25) becomes the overall exponential factor multiplied by the addition of the Lorentzian "delta" functions, which are smoothed by the Lyapunov exponent λ.

In the chaotic billiard systems, the actual weighted power spectrum $\tilde{C}(E)$, which is evaluated from numerically obtained eigen states, is known to have an extremely spiky and oscillatory behavior.[3,7–9] The existence of the scar states in the chaotic billiard systems leads to a relatively smaller amount of selected eigen states contributing dominantly to $A(\mathbf{r})$. The $|c_n|^2$ histograms clearly show this tendency. Figures 4 and 6 show the histograms for Nos. 7 and 14, respectively, where the numbering denotes a specific periodic orbit in the stadium, as shown in Table 1 of Ref. 2.

In Fig. 4, the red curve represents $w(E)$ for No. 7, with $\lambda = 0.418|\mathbf{p}_0|$. The constant 0.418 is the geometric Lyapunov exponent and was evaluated from the monodromy matrix of the corresponding periodic orbit.[2] In addition, ϵ is set to the averaged energy level spacing $\Delta E = 0.0003412 \times 10^4$. Other parameters related to the initial Gaussian are the same as those in Fig. 1. They are simply the

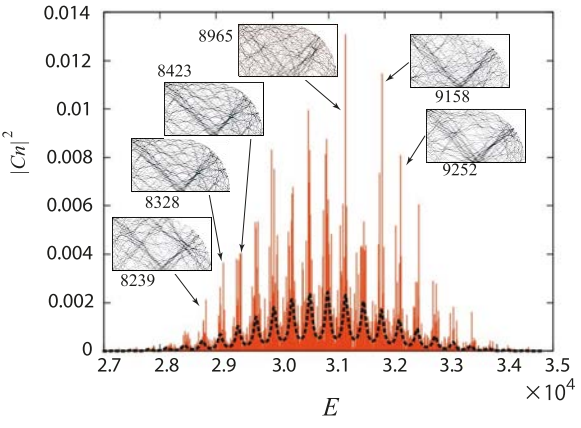

Fig. 4. (Color online) The window function (weighted spectrum) of the Gaussian wavepacket $w(E)$ traveling along orbit No. 7 (a dotted curve) for the case of Fig. 1 (and also Fig. 2) is compared with its expansion coefficients $|c_n|^2$ (bars). The snapshots are shown in Fig. 1 and its $A(\mathbf{r})$ in Fig. 2. Here, the parameters of the initial Gaussian (Eq. (1)) are the same as those in Fig. 1. The insets show the eigen states corresponding to the high peaks. The four-digit numbers near the insets represent the counts from the ground state to the excited states in the insets. The scar states on the classical orbit No. 7 are often observed. The plot of $|c_n|^2$ is extremely spiky; however, it is a typical structure of the "totalitarian" case in Ref. 8.

linear-dynamical predictions of the window function.[3,7–9] The local peaks of the actual weighted spectrum are located at almost equal energy intervals, that is, $\Delta = 0.03193 \times 10^4$, which is very close to the theoretical estimation $\Delta_{\text{th}} = \frac{\hbar}{m}(\frac{2\pi}{L})|\mathbf{p}_0| = 0.03253 \times 10^4$, where $L = 4.8284$ is the length of the specific periodic orbit. Through the semiclassical approximation, the classical action on the classical periodic orbit is determined as $S_r(\xi, \xi; E_0) = \oint_r \mathbf{p} d\mathbf{r} = L\sqrt{2mE_0}$. It must increase by as much as $2\pi\hbar$, adding Δ_{th} to its energy E_0.

As aforementioned, $w(E)$ is less spiky than the actual $|c_n|^2$ histogram. In addition, it is the "totalitarian" case in Ref. 8. In the weighted spectrum of the "totalitarian" system, some particular states have dominant contributions. The scars can often be found in such states. Still, its smoothed behavior follows the estimated envelope function: the window $w(E)$. (The opposite case is called the "egalitarian" in Ref. 8. Then the weighted spectrum essentially follows the window function). It simultaneously allows the emergence of "dynamical scars". Similar to the scar states, if only one primitive periodic orbit has a dominant contribution, the "dynamical scars" become visible. In actuality, the eigen states at peaks often become the scar states of the corresponding periodic orbit (cf. Figs. 4 and 6). Of course, the eigen states with larger c_n would also contribute to the "dynamical scars." However, in some cases, the "dynamical scars" are blurred by the superposition of the other orbits on the eigen state.

The histogram of $|c_n|^2 s$ is extremely spiky, although it is possible to elucidate its smoothed version (Fig. 5) formed by averaging the energy range, which is sufficiently

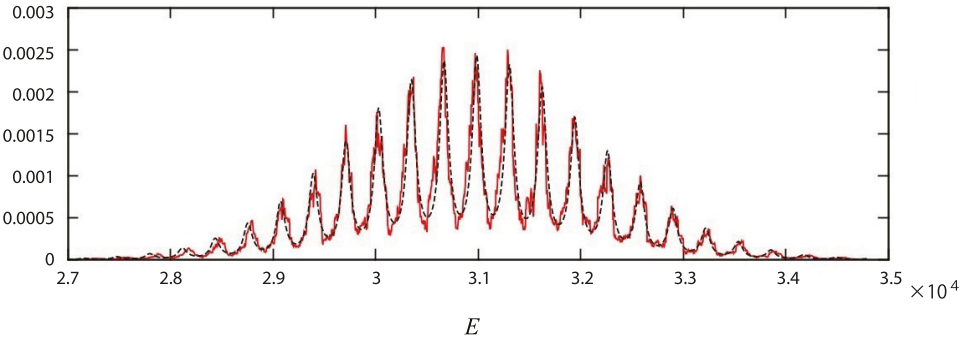

Fig. 5. (Color online) The window function (weighted spectrum) of the Gaussian wavepacket $w(E)$ traveling along orbit No. 7 (a dotted curve) and its averaged behavior of the expansion coefficients $|c_n|^2$ (a solid curve) (cf. Fig. 4). Here, the averaging is performed in the energy range of 20ϵ. The two lines match very closely.

larger than the energy spacing of the levels but much smaller than the required energy. It agrees well with the window function $w(E)$.

The same situation occurs for the periodic orbit No. 14 (Fig. 3(b)). In Fig. 6, the red curve represents $w(E)$, with $\lambda = 0.3684|\mathbf{p}_0|$. The local peaks' energy intervals $\Delta = 0.02340 \times 10^4$ are extremely close to the predicted ones $\Delta_{\text{th}} = \frac{\hbar}{m}(\frac{2\pi}{L})|\mathbf{p}_0| = 0.02428 \times 10^4$ $(L = 6.47)$. Furthermore, other parameters related to the initial Gaussian are the same as those in Fig. 3(b). In addition, the processes in the smoothed histogram are the same as those in the No. 7 orbit case. The smoothed

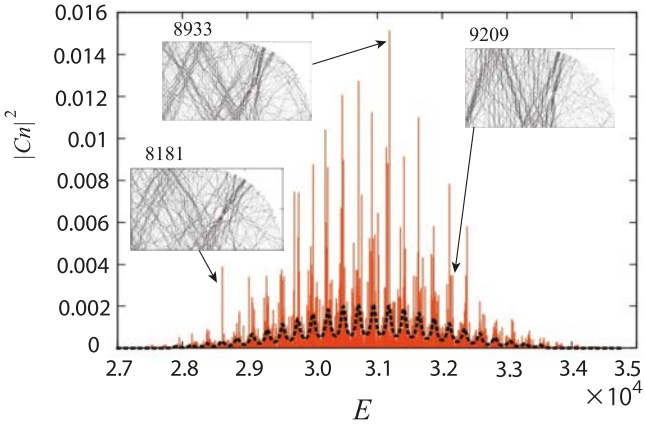

Fig. 6. (Color online) The window function (the weighted spectrum) of the Gaussian wavepacket $w(E)$ traveling along orbit No. 14 (a dotted curve) is compared with its expansion coefficients $|c_n|^2$ (bars). Its $A(\mathbf{r})$ is in Fig. 3(b). Here, the parameters of the initial Gaussian (Eq. (1)) are the same as those in Fig. 3(b). The insets show the eigen states corresponding to the high peaks. The four-digit numbers near the insets represent the counts from the ground state to the excited states in the insets. The scar states on the classical orbit No. 14 are often present. The extremely spiky characteristic feature of this $|c_n|^2$ plot is the same as that in Fig. 4.

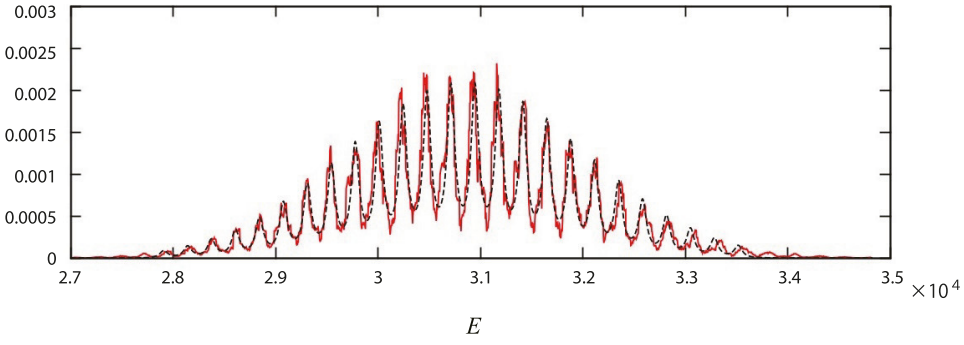

Fig. 7. (Color online) The window function (the weighted spectrum) of the Gaussian wavepacket $w(E)$ traveling along orbit No. 14 (a dotted curve) and the averaged behavior of the expansion coefficients $|c_n|^2$(a solid curve) (cf. Fig. 6). Here, the averaging is performed in the energy range of 20ϵ. The two lines match very closely.

histogram matches very closely with its window function $w(E)$ (Fig. 7). A similar phenomenon occurs for No. 5, which is already published in Ref. 12.

Moreover, the bouncing ball mode produces a considerably unique result (Fig. 8). This exceptional mode is the only nonchaotic periodic orbit in the stadium billiard. It has a zero Lyapunov exponent and no chaotic origin because it bounces between the parallel walls of the billiard in terms of classical mechanics. However, the parameter λ still cannot be set to zero or be infinitesimally small in our numerical calculation because the Lorentzian approaches the Dirac delta function in such a limit; this cannot be presented exactly in numerical calculation. The numerical results clarify that only the wave functions with scars on the bouncing ball mode significantly contribute to the "dynamical scar." Figure 9 compares the numerical histogram and the estimated weighted spectrum, both of which show strikingly good agreement. Numerically calculated interval between the peaks is $\Delta = 0.07524$, whereas its theoretical estimation is $\Delta_{\text{th}} = \frac{\hbar}{m}(\frac{2\pi}{L})|p_0| = 0.07854$ $(L = 2)$. Note that the width of the sharp peaks λ in the weighted spectrum is replaced by the averaged level

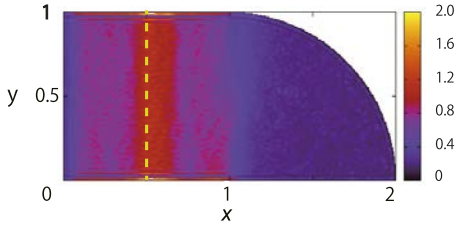

Fig. 8. (Color online) The time-average of the evolving wavepacket $A(\mathbf{r})$ on the bouncing ball mode of the stadium billiard. It corresponds to orbit No. 1. The initial Gaussian wavepacket is set as $|\mathbf{p}_0| = 250$ and $\sigma_0 = 0.15$. The wavepacket is launched from $(1/2, \sqrt{3}/4)$ and the launching angle is $\theta = \pi/2$. The broken yellow line corresponds to the classical periodic orbit. It belongs to the one-parameter family of the bouncing ball mode, whose members bounce up and down between two parallel straight sections of the boundary infinitely, and the launching point is on the line.

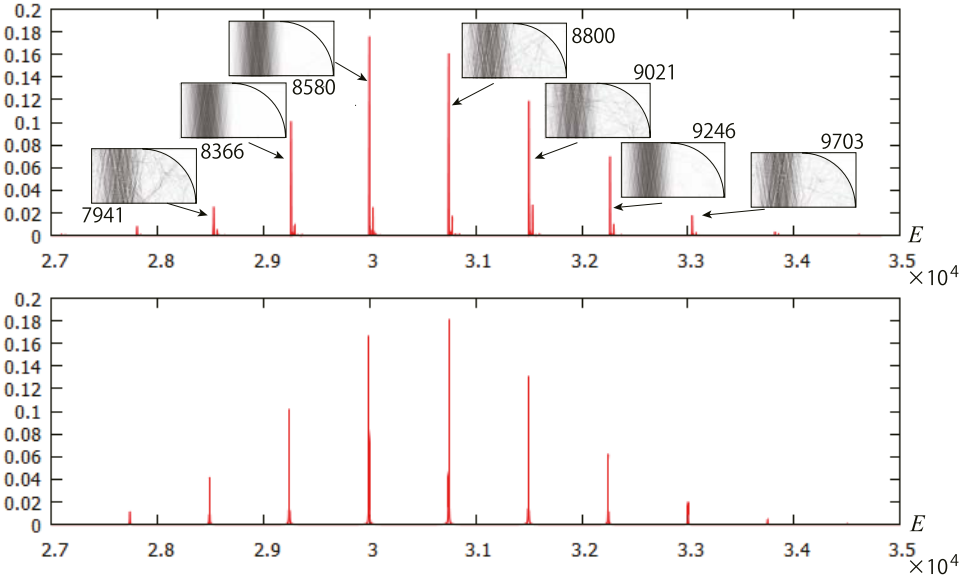

Fig. 9. (Color online) Expansion coefficients $|c_n|^2$ (upper graph) and window function (the weighted spectrum) of the Gaussian wavepacket $w(E)$ (lower graph) for the bouncing ball mode. These graphs are almost identical. The four-digit numbers near the insets represent the counts from the ground state to the excited states. The parameters of the wavepacket are the same as those in Fig. 8.

spacing $\overline{\Delta E}$, instead of the theoretically exact value of the vanishing Lyapunov exponent $\lambda = 0$. It also implies that this system does not have finer energy resolution than $\overline{\Delta E}$.

As mentioned earlier, with a good agreement between $w(E)$ and the averaged behavior of $|c_n|^2$, the semiclassical approximation can be expected to function satisfactorily in this field. Moreover, it reminds us of the "totalitarian" aspect of the system.

If we choose a sufficiently small window size to reasonably assume that only one eigen state would be in the window simultaneously, it essentially resembles the result of Ref. 2 for the scar states. However, in this study, the window size is much larger because the initial wavepacket must involve the contribution of the eigen states in a broader energy range. Thus, a scar is not directly observed in the snapshot of the time-dependent wave functions (Fig. 1(f)). The "dynamical scar" is the superposition of many corresponding states in the energy window.

5. Semiclassical Approximation

Through semiclassical approximation,[2] the localization becomes the summation of two parts:

$$A(\mathbf{r}) \cong \langle \rho_0(\mathbf{r}, E) \rangle + \int w(E) \mathrm{Im} G_{\mathrm{osc}}(\mathbf{r}, \mathbf{r}; E) dE = \langle \rho_0(\mathbf{r}, E) \rangle + A_{\mathrm{osc}}(\mathbf{r}), \tag{26}$$

where

$$G_{\rm osc}(\mathbf{r},\mathbf{r};E) \cong \frac{2}{(2\pi)^{1/2}\hbar^{3/2}} \times \sum_{\gamma,n} \frac{D_{\gamma,n}(\xi)^{1/2}}{v} \left\{ \exp\left[\frac{i}{\hbar} \left(S_{\gamma,n}(\xi,\xi;E) + \frac{W_{\gamma,n}(\xi)}{2}\eta^2 \right) \right] - i\frac{\pi\nu_{\gamma,n}}{2} - i\frac{3}{4}\pi \right\}. \quad (27)$$

The first term of Eq. (26) on the right-hand side is the smooth part $\langle \rho_0 \rangle$, and the second is the oscillatory term $A_{\rm osc}$. Further, the angle brackets $\langle \cdots \rangle$ denote an average over the energy range that the window function $w(E)$ covers, and $\rho_0(\mathbf{r},E)$ is the classical probability density of finding a particle with energy E at point $\mathbf{r}$. Needless to say, $w(E)$ depends on the shape of the (initial) wavepacket. The ξ axis is set along the concerned periodic orbit, and the η axis perpendicular to it at point ξ. The classical action of the n-fold repeated orbit can be derived as $S_{\gamma,n} = nS_\gamma$ from the action of the primitive orbit γ: S_γ. Then, $T_{\gamma,n}(\mathbf{r},E) = nT_\gamma$, T_γ is the period of the primitive orbit γ. Its maximal number of conjugate points $\nu_{\gamma,n} = n\nu_\gamma$ can be derived from the primitive ν_γ. In addition, $W_{\gamma,n}(\xi)$, $D_{\gamma,n}(\xi)$ are the versions for the n-fold periodic orbit and can be expressed as $D_\gamma = -(\frac{\partial^2 S_\gamma}{\partial\eta'\partial\eta''})_{\eta'=\eta''=0}$ and $W_\gamma(\xi) = (\frac{\partial^2 S_\gamma}{\partial\eta'^2} + \frac{\partial^2 S_\gamma}{\partial\eta'\partial\eta''} + \frac{\partial^2 S_\gamma}{\partial\eta''^2})_{\eta'=\eta''=0}$ for the primitive orbit. They can be derived from D_γ: $D_{\gamma,n}(\xi) = D_\gamma \frac{\mu_1-\mu_2}{\mu_1^n-\mu_2^n}$, $W_{\gamma,n}(\xi) = D_{\gamma,n}(\mu_1^n+\mu_2^n-2)$. Note that μ_1, $\mu_2 = \mu_1^{-1}$ are the eigenvalues of the monodromy matrix of the primitive orbit.

It is assumed that only one specific periodic orbit $\gamma = C$ shows a prime contribution. Moreover, the primitive orbit $n = 1$ is expected to be dominant on the periodic orbit because the factor $D_{C,n}$ vanishes rapidly with increasing n. Therefore, the oscillatory part of A can be approximated on the classical orbit C ($\eta = 0$) as

$$A_{\rm osc}(\xi) \cong \frac{2\sqrt{2}}{\pi\hbar^{7/2}} \frac{\sigma_0}{v} \epsilon\Delta \sum_j \exp\left[-\frac{{\sigma_0}^2}{\hbar^2 v^2}(E_j - E_0)^2 \right] \frac{|D_C|^{1/2}}{v} \times \int \frac{1}{\pi} \frac{\lambda/2}{\{(E-E_j)/\hbar\}^2 + (\lambda/2)^2} {\rm Im}\left\{ i \exp\left[\frac{i}{\hbar} S_C - i\frac{\pi}{2}\nu_C + i\pi N_C - i\frac{1}{4}\pi \right] \right\} dE. \quad (28)$$

Note that N_C is the number of hits on the boundary, when a particle travels around the closed orbit C, and $D_C = D_{C,1}$. Under the semiclassical approximation, at $E = E_j$, it can be well assumed that $\exp\{\frac{i}{\hbar}S_C(\xi,\xi;E_j) - i\frac{\pi}{2}\nu_C + i\pi N_C - i\frac{1}{4}\pi\} = 1$. Finally, integration in Eq. (28) can be performed using a complex integral, and the localization is evaluated as

$$A(\xi) = \langle\rho\rangle + A_{\rm osc}(\xi) = \frac{1}{\rm Area} + \frac{2\sqrt{2}}{\pi\hbar^{5/2}} \frac{\sigma_0}{v} \epsilon\Delta \frac{|D_C(\xi)|^{1/2}}{v} \sum_j \exp\left[-\frac{{\sigma_0}^2}{\hbar^2 v^2}(E_j - E_0)^2 \right] e^{-T_j\frac{\lambda}{2}}, \quad (29)$$

where $S_C(\xi,\xi;E_j + i\frac{\hbar\lambda}{2}) \cong S_C(\xi,\xi;E_j) + iT_j\frac{\lambda\hbar}{2}$ is used, T_j is the period of the periodic orbit at $E = E_j$, and Area is the area of the billiard. Finally, the averaged level

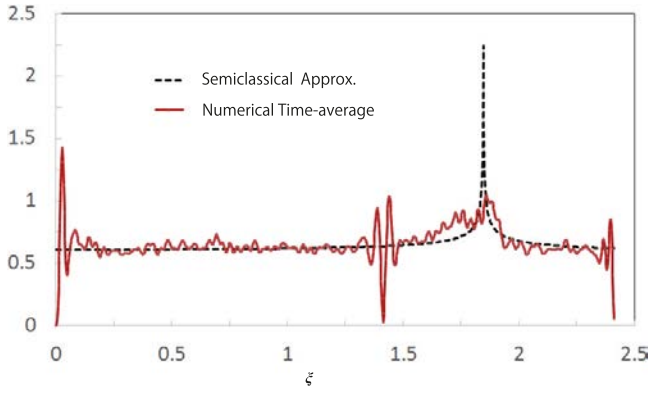

Fig. 10. (Color online) Comparison of the semiclassically approximated time-average of the evolving wavepacket (29) on the periodic orbit No. 7 (a dotted curve) and its numerically calculated localization (a solid curve). They are presented as functions of the distance ξ from the point (0,1), which is measured along the broken yellow line in Fig. 2. At a distance $\xi_C = \sqrt{2+\sqrt{2}} = 1.8478\ldots$, the semiclassical approximation diverges. At distances 0, $\sqrt{2} = 1.4142\ldots$, and $1+\sqrt{2} = 2.4142\ldots$, the boundary walls are present. At the boundary, the wave function becomes zero and shows a peculiar rough wavy behavior.

spacing $\overline{\Delta E}$, which is the criterion of the energy resolution limit of the billiard system, is adopted for ϵ.

The evaluated localization A on the periodic orbit No. 7 (Fig. 2) is presented in Fig. 10. Assuming that the wave function is completely flat in the finite region, $\langle\rho\rangle$ must be the inverse of the area of the billiard: $\{(4+\pi)/4\}^{-1} = 0.5601\ldots$ throughout the stadium. Owing to the scar or the contribution of the classical periodic orbit, the concentration enhances the absolute square of the wave function by at least 10% on the periodic orbit above the average behavior $\langle\rho\rangle$, except in the neighborhood of the singularity around the conjugate point. Of course, it cannot recreate the wavy behavior, which is particularly sharp close to the boundary because Eq. (29) does not show the exact effect of the boundary condition. The approximation is determined essentially through the length of the orbits and the energy. Actually, the wave must be zero at the boundary according to the Dirichlet condition, and all dominant eigenfunctions' phases become almost coherent near the boundary. Figure 11 shows the semiclassical approximation of No. 14. In addition, it presents essentially the same results as No. 7 (Fig. 10).

The singularity at the conjugate point is inevitable for the semiclassical approximation; however, it is also beyond the scope of the approximation in the neighborhood of the point. The semiclassical approximation of the wave function diverges at the point due to the factor $D_C = 1/m_{12}$, and m_{12} is the off-diagonal element of the monodromy matrix[2] for the unstable classical periodic orbit C. In our study, $m_{12} = -2\{(2+\sqrt{2}) - \xi^2\}$ for No. 7 (Fig. 10), and $m_{12} = -2\{(5+\sqrt{5}) - \xi^2\}$ for No. 14 (Fig. 11). In both cases, ξ is measured from the left wall and along the orbits. The monodromy matrix element m_{12} becomes zero and D_C diverges at the conjugate point ξ_C, where the classical orbits near the classical periodic orbit converge. The

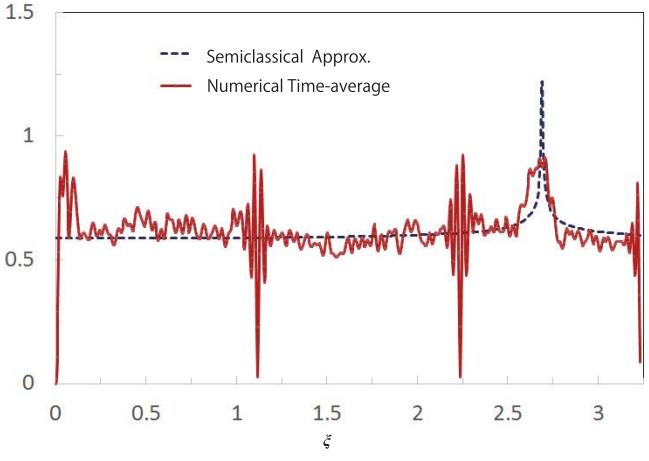

Fig. 11. (Color online) Comparison of the semiclassically approximated time-average of the evolving wavepacket (29) on the periodic orbit No. 14 (a dotted curve) and its numerically calculated localization (a solid curve). They are presented as functions of the distance ξ from the point (0,0), which is measured along the broken yellow line in Fig. 3(b). At a distance $\xi_C = \sqrt{5+\sqrt{5}} = 2.6900\ldots$, the semiclassical approximation diverges. At distances 0, $\frac{\sqrt{5}}{2} = 1.1180\ldots$, $\sqrt{5} = 2.2361\ldots$, and $1+\sqrt{5} = 3.2361\ldots$, the boundary walls exist. At the boundary, the wave function becomes zero and shows a peculiar rough wavy behavior.

conjugate points are located at $\xi_C = \sqrt{2+\sqrt{2}}$ for No. 7 measured from the point $(0,1)$, and $\sqrt{5+\sqrt{5}}$ for No. 14 measured from $(0,0)$. In reality, a relatively strong enhancement exists around the point. Apart from these properties, the semiclassical approximation works well, and Eq. (29) still matches remarkably with the numerically evaluated time-averages on the orbits.

6. Conclusion

The quantum phenomenon, the "dynamical scar", is analyzed from the aspect of the eigen state expansion of the incident wavepacket and the semiclassical approximation. By launching a Gaussian wavepacket along a classical unstable periodic orbit, its weighted power spectrum $\bar{C}(E)$ accomplishes a good match with its averaged histogram of expansion coefficients $|c_n|^2$.

By utilizing $\bar{C}(E)$ as the energy window function for the semiclassical approximation, the "dynamical scars" can be evaluated. The periodic orbit critically contributes to the approximation. However, it has nonrealistic singularities close to the conjugate points on the orbit. The window function $w(E)$, which is manipulated from $\tilde{C}(E)$, plays a crucial role for the approximation.

References

1. E. J. Heller, *Phys. Rev. Lett.* **53**, 1515 (1984).
2. E. B. Bogomolny, *Phys. D* **31**, 169 (1988).

3. E. J. Heller, Wavepacket dynamics and quantum chaology, in *Chaos and Quantum Physics*, eds. M. J. Giannoni, A. Voros and J. Zinn-Justin, Les Houches Session LII, 1989 (Elsevier, Amsterdam, 1991), p. 547.
4. M. V. Berry, *Proc. R. Soc. Lond. A* **423**, 219 (1989).
5. E. J. Heller, *Phys. Rev. A* **35**, 1360 (1987).
6. S. Tomsovic and E. J. Heller, *Phys. Rev. Lett.* **70**, 1405 (1993).
7. S. Tomsovic and E. J. Heller, *Phys. Rev. E* **47**, 282 (1993).
8. L. Kaplan and E. J. Heller, *Ann. Phys. (N.Y.)* **264**, 171 (1998).
9. L. Kaplan and E. J. Heller, *Phys. Rev. E* **62**, 409 (2000).
10. H. Tsuyuki, M. Tomiya, S. Sakamoto and M. Nishikawa, *Surf. Sci. Nanotech.* **7**, 721 (2009).
11. M. Tomiya, H. Tsuyuki and S. Sakamoto, *Commun. Comp. Phys.* **182**, 245 (2011).
12. M. Tomiya, H. Tsuyuki, K. Kawamura, S. Sakamoto and E. Heller, *J. Phys. Conf. Ser.* **640**, 012068 (2015).
13. H.-J. Stöckmann, Applications of periodic orbit theory, in *Quantum Chaos an Introduction* (Cambridge University Press, Cambridge, 1999), p. 305.
14. L. A. Bunimovich, *Funct. Anal. Appl.* **8**, 254 (1974).
15. M. V. Berry, *Proc. R. Soc. Lond. A* **400**, 229 (1985).